Available online at www.sciencedirect.com
ScienceDirect
Journal of Catalysis 249 (2007) 278–288
JOURNAL OF CATALYSIS
www.elsevier.com/locate/jcat

Characterization and catalytic behavior of highly active tungsten-doped SBA-15 catalyst in the synthesis of glutaraldehyde using an anhydrous approach

Xin-Li Yang [a,b], Wei-Lin Dai [a,*], Ruihua Gao [a], Kangnian Fan [a,*]

[a] *Department of Chemistry and Shanghai Key Laboratory of Molecular Catalysis and Innovative Materials, Fudan University, Shanghai 200433, PR China*
[b] *School of Chemistry & Chemical Engineering, Henan University of Technology, Henan 450052, PR China*

Received 8 November 2006; revised 29 April 2007; accepted 3 May 2007

Available online 19 June 2007

Abstract

Tungsten-doped ordered SBA-15 prepared by the in situ synthesis method was systematically characterized by UV-Raman, UV–vis DRS, FT-IR, XPS, and H_2-TPR. It was found that the dispersion and nature of the tungsten species depend strongly on the tungsten oxide content. The tungsten species are located mainly in isolated tetrahedral or low-condensed oligomeric environments, and there are strong interaction between tungsten species and the silica-based matrix at tungsten oxide content <20 wt%. Higher tungsten oxide content leads to the formation of bulk tungsten species. It was also found that the ordered hexagonal mesoporous structure of SBA-15 is retained, and strong Brønsted and Lewis acid sites are formed on tungsten incorporation. The superior catalytic performance in the selective oxidation of cyclopentene has been attributed to its proper content of tungsten species, high dispersion, and strong surface acidity.

Keywords: Cyclopentene; Glutaraldehyde; Hydrogen peroxide; Tungsten species; SBA-15; W-doped SBA-15

1. Introduction

The synthesis of siliceous mesoporous materials has attracted great interest because it extends the range of molecular-sieve materials into the very-large pore regime [1]. The incorporation of transition metal ions in these mesoporous structures is a very useful method for providing this material with potential catalytic applications. SBA-15, a new type of ordered mesoporous material appearing after the M41S series, is synthesized with triblock copolymers as structure-directing agents under strongly acidic conditions. It has a high surface area (600–1000 $m^2\,g^{-1}$), thick walls, and uniform tubular channels with tunable pore diameters in the range of 5–30 nm, significantly larger and with higher hydrothermal stability than those of MCM-41 [2,3]. Thus, it has attracted great attention in the field of catalysis. Tungsten is one of the most-studied transition metal ions (along with as Al [4], Ti [5], V [6], and Sn [7]) incorporated into SBA-15, due to its interesting catalytic properties in many reactions. Tungsten is widely used for the metathesis and isomerization of alkenes [8], selective oxidation of unsaturated compounds [9], dehydrogenation of alcohols [10], and hydrodesulfurization and hydrocracking of heavy fractions in the petroleum chemistry [11,12], the subject most heavily researched. In addition, research groups have attempted to synthesize mesoporous tungsten oxide materials [13] or incorporate tungsten into nonsiliceous mesostructured materials (TiO_2) [14,15] and siliceous mesoporous molecular sieves (e.g., silica, M41S, SBA-n) by impregnation [16], cogelation [17], insertion [18–20], or grafting [21]. In these materials, the structure of the nonsupported tungsten oxide mesoporous materials is not stable and will collapse on calcination. Thus, incorporating tungsten into nonsiliceous or siliceous mesoporous materials has attracted considerable interest because of their diverse compositions that lead to potential applications in catalysis. Our group has reported studies on the synthesis and catalytic performance of core–shell mesoporous-structured WO_3/TiO_2

* Corresponding authors. Fax: +86 21 65642978.
E-mail addresses: wldai@fudan.edu.cn (W.-L. Dai), knfan@fudan.edu.cn (K. Fan).

0021-9517/$ – see front matter
doi:10.1016/j.jcat.2007.05.002

spheroids and tungsten-doped siliceous mesoporous molecular sieve materials, which show good catalytic activity in the selective oxidation of cyclopentene with aqueous H_2O_2 [15,20]. Other previous studies [16–21] have shown that the dispersion of tungsten oxide and its oxidation state, surface acidity, and structure strongly depend on the preparation methods, the tungsten precursors, and the nature of the support. In turn, all of these factors are likely to affect the catalytic properties. The industrial importance of the silica–tungsten oxide system has sparked numerous studies of their properties and catalytic applications.

In a preliminary research note [22], for the first time we reported the synthesis of a novel tungsten-doped SBA-15 catalyst by the in situ synthesis method, which showed excellent catalytic performance in the production of glutaraldehyde (GA) by anhydrous hydrogen peroxide from cyclopentene (CPE) in the presence of tributyl phosphate (TBP). GA is used extensively in disinfection and sterilization. An important way to produce GA is through the selective oxidation of CPE, because a great quantity of CPE can be easily obtained by the selective hydrogenation of cyclopentadiene, which can be readily obtained from the decomposition of dicyclopentadiene, a main byproduct of the C-5 fraction in the petrochemical or coking industry [23,24]. The superior performance of tungsten-doped SBA-15 catalyst is related to the high surface concentration of WO_x species dispersed on well-ordered hexagonal pore walls of the SBA-15 support. Nonetheless, a fundamental understanding of the dispersion, coordination, reducibility, and oxidation state of the WO_x species and the surface acidity of the catalyst remain unclear.

To gain more insight into the nature and the redox properties of the tungsten-doped SBA-15 catalysts, and also to explore the possible relationship between the reaction mechanism and the catalyst properties, the present work systematically characterized the tungsten-doped SBA-15 catalysts by various analytical and spectroscopic techniques, including UV-Raman, XPS, FT-IR, and H_2-TPR, and investigated their catalytic performance in the selective oxidation of CPE in the anhydrous H_2O_2/TBP system.

2. Experimental

2.1. Catalyst preparation

A typical procedure for the synthesis of W-doped SBA-15 catalyst was as follows. First, 5 g of Pluronic P123 triblock polymer ($EO_{20}PO_{70}EO_{20}$, $Mav = 5800$, Aldrich) and 28 g of distilled water were added to 150 mL of 2 M HCl and stirred for 4 h at 313 K. Then 10 g of $Si(OC_2H_5)_4$(TEOS) was added to this mixture and stirred for 30 min. Then 13 mL of an aqueous solution of sodium tungstate ($Na_2WO_4{\cdot}2H_2O$, 0.2 M) was added. The mixture was aged at 313 K under moderate stirring for 24 h, and then crystallized at 368 K for 3 days. The solid product was filtered, washed with distilled water, and dried at room temperature. Finally, it was calcined at 873 K in air for 5 h to remove the template and used as a catalyst with no further treatment.

2.2. Characterizations

The UV-Raman measurements were carried out on a confocal microprobe Jobin Yvon LabRam Infinity Raman system using the UV line at 325 nm from a Kimmon IK3201R-F He–Cd laser as the exciting source. The laser output was 30 mW, and the maximum incident power at the sample was approximately 6 mW.

UV–vis DR spectra were collected on a Shimadzu UV-2540 spectrometer with $BaSO_4$ as a reference. The XPS spectra were recorded on a Perkin-Elmer PHI 5000C ESCA system equipped with a dual X-ray source, using the Al$K\alpha$ (1486.6 eV) anode and a hemispherical energy analyzer. The background pressure during data acquisition was kept below 10^{-6} Pa. Measurements were performed at pass energy of 93.90 eV to ensure sufficient sensitivity for the acquisition scan, and a pass energy of 23.50 eV was used for the scanning of the narrow spectra of Si_{2p}, W_{4f}, O_{1s}, and C_{1s} to ensure sufficient resolution. All binding energies were calibrated using contaminant carbon (C_{1s} = 284.6 eV) as a reference.

The surface acidity was monitored from the FT-IR spectra recorded after the adsorption of pyridine, using a Bruker Vector 22 spectrometer coupled to a conventional high-vacuum system. The sample was compacted to a self-supporting wafer and calcined at 673 K for 1 h in an in situ IR gas cell under vacuum before pyridine adsorption [25]. Pyridine was adsorbed at room temperature from an argon flow containing 2 vol% pyridine. Then the samples were heated to 373 K and evacuated to remove physisorbed and weakly chemisorbed pyridine. Temperature-programmed desorption of the adsorbed pyridine starting at 373 K was studied by stepwise heating of the sample under vacuum to characterize the types and strengths of the acid sites. Difference spectra were obtained by subtracting the background (base spectrum) of the unloaded sample.

TPR analysis was carried out on a homemade apparatus loaded with 100 mg of catalyst. The samples were pretreated in flowing air at 873 K for 2 h to ensure complete oxidation. Then the samples were subsequently contacted with H_2/Ar mixture (H_2/Ar molar ratio of 5/95 and a total flow of 40 mL min^{-1}) and heated at a ramp rate of 10 K min^{-1} to a final temperature of 1273 K. H_2 consumption was monitored using a TCD detector. The tungsten content was determined by ICP (IRIS Intrepid, Thermo Elemental Company) after solubilization of the samples in HF:HCl solutions.

2.3. Activity test

The activity test was performed at 308 K for 12 h with magnetic stirring in a closed 100-mL regular glass reactor using anhydrous hydrogen peroxide as the oxygen donor and TBP as the solvent. The quantitative analysis of the reaction products was performed by gas chromatography (GC) method, and identification of different products in the reaction mixture was determined by GC–mass spectrometry (GC–MS), as described previously [20,26].

3. Results and discussion

3.1. Characterization of the tungsten-doped SBA-15 catalyst

The tungsten-doped SBA-15 catalysts were systematically characterized by various analytical and spectroscopic techniques. XRD and SEM/TEM results show that a suitable weight content (<20%) is needed to obtain a high dispersion of WO_x species and maintain the typical mesoporous structure of the W-doped SBA-15 catalysts. More detailed information on XRD and SEM/TEM is given in the supporting materials. Other characterization results are discussed herein.

3.1.1. UV–vis DRS

To obtain information of the chemical nature and coordination states of tungsten oxide species, diffuse reflectance spectra in the UV–vis region of W-doped SBA-15 samples were recorded; these are shown in Fig. 1. This method is known to be highly sensitive for distinguishing species between incorporated metal and extra-framework metal oxides in different mesostructures [27,28]. For comparison, the UV–vis DR spectra of sodium tungstate ($Na_2WO_4{\cdot}2H_2O$) and bulk WO_3 are also shown in Fig. 1. The spectrum of sodium tungstate, with a spinel structure and isolated $[WO_4]^{2-}$ tetrahedra, is characterized by a maximum at 230 nm (curve a) [19,29]. For pure siliceous SBA-15, there are no evident bands in the spectrum (not shown here); after introduction of tungsten oxide into SBA-15, three Raman bands appear at 230, 290, and 430 nm. The broad band at about 430 nm of the 30 wt% W-doped SBA-15 and impregnated 20 wt% WO_3/SBA-15 sample (curves d and e) can be attributed to tungsten trioxide by comparison with the spectrum of bulk WO_3 (curve f) [19,30]. The second broad band at about 290 nm presents another kind of tungsten oxide species. Weber et al. showed that the low-energy absorption is shifted toward a lower wavelength with decreasing nuclearity of molybdenum or tungsten entities [31,32]. Therefore, this broad band should be assigned to isolated tungsten species or low-condensed oligomeric tungsten oxide species. The sharp band at 230 nm of the in situ synthesized samples (curves b–d) can be attributed to isolated $[WO_4]$ tetrahedral species by comparison with the structure of sodium tungstate. The absence of the broad band at 430 nm may reflect the fact that the tungsten oxide species are highly dispersed and no crystalline WO_3 is formed in W-doped SBA-15 samples with tungsten oxide content <20 wt% (curve b). There is a weak band at 430 nm for the 20 wt% W-doped SBA-15 sample, indicating formation of only a small amount of low-crystalline WO_3 species, which is in line with the result from wide-angle XRD. Further increasing the tungsten oxide content up to 30 wt% will lead to the formation of a large quantity of crystalline WO_3 species, resulting in the appearance of strong bands at 430 nm, which can be also confirmed by the TEM images and the crystalline phase of WO_3 detected by XRD (see the supporting materials). The UV–vis DR spectra further demonstrate that high dispersion of the tungsten oxide species is essential to the high catalytic performance of the as-synthesized catalysts, as discussed below.

3.1.2. UV-Raman

UV-Raman spectroscopy is an important technique for identifying incorporated framework transition metal ions in metal-containing zeolites [33] and MCM-41 materials [34]. UV-Raman spectroscopy has no fluorescence background to be corrected as is commonly present in most visible Raman spectra, thus greatly improving its sensitivity and resolution. Furthermore, the resonance Raman effects can selectively enhance the Raman bands that are directly associated with the framework metallic ion while keeping the remaining Raman bands unchanged for metal-containing molecular zeolites. The UV-Raman spectra of various samples, shown in Fig. 2, are significantly different than the visible Raman spectra, as reported previously [22]. No bands attributed to the tungsten oxide

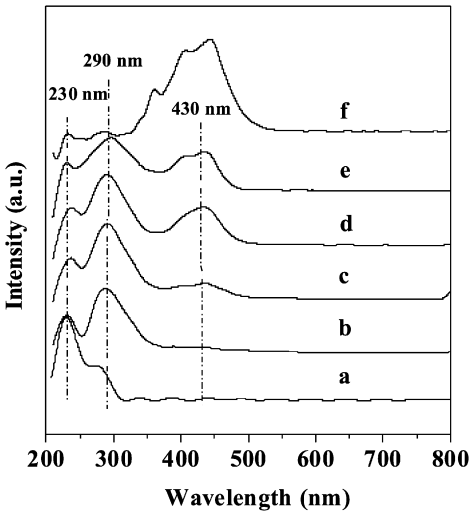

Fig. 1. UV–vis diffuse reflectance spectra of various samples after dehydration at 673 K in air for 2 h: (a) $Na_2WO_4{\cdot}2H_2O$; (b) 10 wt% WO_3-SBA-15; (c) 20 wt% WO_3-SBA-15; (d) 30 wt% WO_3-SBA-15; (e) 20 wt% WO_3/SBA-15; (f) bulk WO_3.

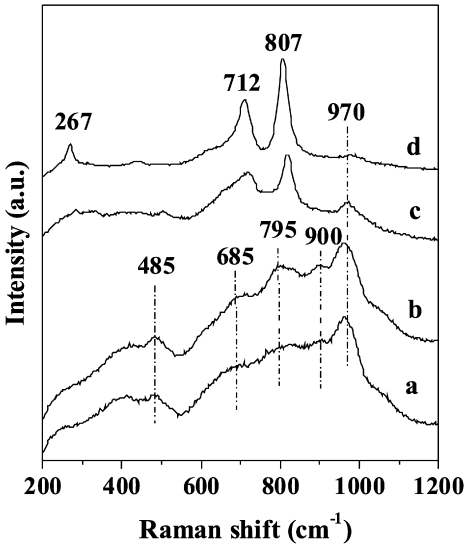

Fig. 2. UV-Raman spectra of various samples: (a) 10 wt% WO_3-SBA-15; (b) 20 wt% WO_3-SBA-15; (c) 30 wt% WO_3-SBA-15; (d) 20 wt% WO_3/SBA-15.

species or the siliceous SBA-15 structure can be observed for the W-doped SBA-15 samples ($WO_3 \leqslant 20$ wt% [22]); however, new Raman bands at 485, 685, 795, 900, and 970 cm^{-1} are observed for those samples with WO_3 content <20 wt% from the UV-Raman spectra (Fig. 2, a and b). The bands at 485 and 795 cm^{-1} are associated with the vibration of the siliceous SBA-15 matrix [19,34]. The band at 970 cm^{-1} is assigned to the symmetric stretching mode of the terminal W=O bond of the tetrahedrally coordinated tungsten oxide species [19,35,36], which has been suggested as the active site of the tungsten-based catalysts [37]. The Raman band at about 900 cm^{-1} has been used to characterize the incorporation of the transition metal ions in the silica framework as the Si–O– or $Si(–O–)_2$ functionalities perturbed by the neighboring metal ions, such as V [38] and W [35]. The presence of the Raman band at about 900 cm^{-1} is also a typical evidence for the isomorphous substitution of silicon by tungsten in the tungsten-doped SBA-15 samples. The band at 685 cm^{-1} may be assigned to stretching and bending modes of W–O bonds in the low condensed polymeric WO_x species, in comparison with the UV-Raman bands of crystalline WO_3 (Fig. 2, c and d) [39]. For the 30 wt% W-doped SBA-15 and the traditional impregnated 20 wt% WO_3/SBA-15 sample, the characteristic bands of siliceous SBA-15 matrix vanished because of the very strong UV-Raman bands of crystalline WO_3, indicating the formation of a very poorly dispersed tungsten oxides.

3.1.3. TPR

TPR profiles of the various samples and the bulk WO_3 are compared in Fig. 3. The bare siliceous SBA-15 shows no reduction peak in the temperature range investigated here (Fig. 3a), whereas the TPR profile of bulk WO_3 exhibits three main peaks with maxima at 903, 1063, and 1183 K (Fig. 3e). These peaks may be assigned to the three-stepwise reduction of WO_3 to W(0) (WO_3(VI) → $WO_{2.9}$(V,VI) → WO_2(IV) → W(0)) [40,41]. The two higher temperature peaks at 1063 and 1183 K are associated with the reduction of W(VI) species in the tetrahedral coordination [40], whereas the peak at lower temperature (903 K) is correlated with the reduction of the supported WO_3 crystallites [42]. Furthermore, Horsley et al. [43] found that the isolated and the low-condensed oligomeric tungsten oxide species (e.g., dipolymer) cannot be easily reduced. The reduction of the W-doped SBA-15 samples strongly depends on the content and dispersion of WO_3. A shift of the TPR profiles to lower temperatures is observed when increasing the WO_3 content from 10 to 30 wt%, until the reduction behavior is close to that of bulk WO_3 on the 30 wt% sample. The existence of a single H_2 consumption peak for the 10 and 20 wt% samples at about 1210 K may indicate the high dispersion of the tungsten oxide species, which can be assigned to the reduction of tetrahedrally coordinated species or the low-condensed oligomeric tungsten oxide species [42,43], whereas the TPR profile of the 30 wt% sample is similar to that of bulk WO_3, demonstrating the presence of crystalline WO_3 in the 30 wt% sample. de Lucas et al. [44] reported that the reducibility of the tungsten-based silica catalysts increases as the strength of the interaction of metal oxide species with the support surface decreases. Therefore, it can be concluded that the interaction between the high-dispersive tungsten oxide species and the SBA-15 framework is very strong, thus reducing the leaching of tungsten species into the reaction mixture compared with the supported counterparts.

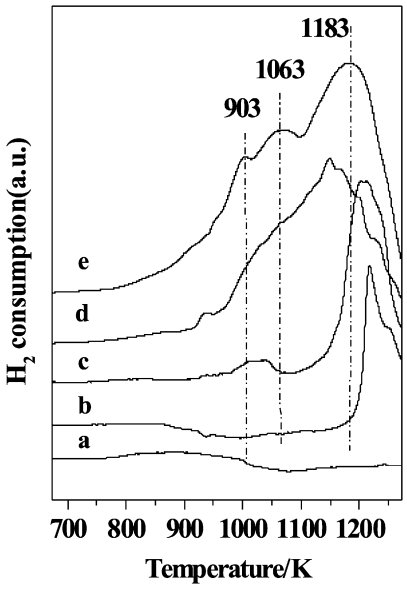

Fig. 3. Temperature-programmed reduction profiles of different samples: (a) SBA-15; (b) 10 wt% WO_3-SBA-15; (c) 20 wt% WO_3-SBA-15; (d) 30 wt% WO_3-SBA-15; (e) bulk WO_3.

3.1.4. Py-FT-IR

Pyridine adsorption measured by IR spectroscopy was used to evaluate the strength and types of acid sites of the W-doped SBA-15 samples. Fig. 4 shows the FT-IR spectra of the bare SBA-15 and 20 wt% tungsten-doped SBA-15 samples recorded after the adsorption of pyridine and subsequent evacuation at 423, 473, 573, and 673 K. The Py-FT-IR spectrum recorded after adsorption of pyridine at room temperature on the bare SBA-15 shows bands at 1595 and 1445 cm^{-1}, ascribed to pyridine coordinately bonded to weak surface Lewis acid sites (Fig. 4A) [45], which vanish almost completely after outgassing at 473 K. In addition to bands at 1595 and 1445 cm^{-1}, the spectrum recorded for the 20 wt% tungsten-doped SBA-15 sample shows bands at 1488, 1545, and 1635 cm^{-1} due to protonated pyridine bonded to surface Brønsted acid sites, indicating that the presence of tungsten-doped species leads to the development of surface Brønsted acid sites (Fig. 4B) [16]. The intensities of all of these bands decrease after outgassing at increasing temperatures, but they are still recorded even after outgassing at 573 K, illustrating that both types of acid sites are rather strong and are related to tungsten oxide incorporation. Similar spectra are recorded for samples of 10 and 30 wt% tungsten-doped SBA-15 (not shown here), but the number of the Lewis and Brønsted acid sites increases with the increment of the tungsten oxide contents up to 20 wt%. For the 10 wt% sample, all of these bands almost disappear after outgassing at 573 K, which may be associated with the much more uncovered silica surface [16]. When the tungsten oxide content is increased to 20 wt%, the surface concentration of the Lewis and Brønsted

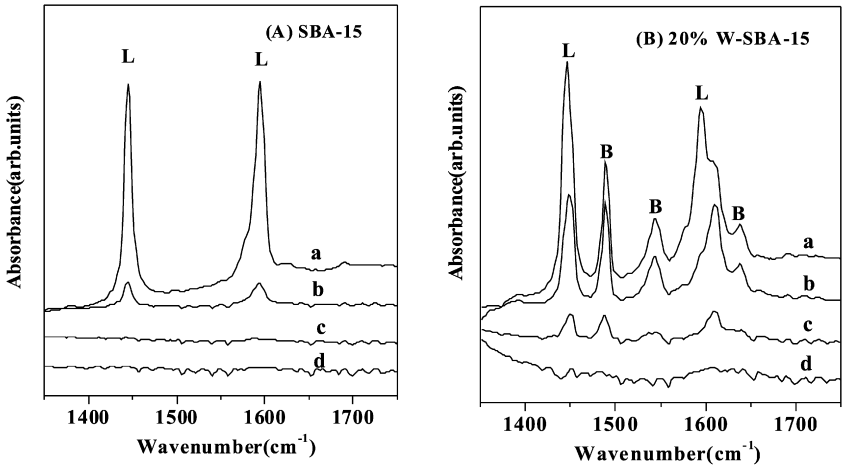

Fig. 4. FT-IR spectra of pyridine adsorbed on the sample recorded at different temperatures: (a) 423, (b) 473, (c) 573, and (d) 673 K.

acid sites increases, possibly due to an increase in the surface concentration of tungsten oxide species covering more silica surface and the high dispersion of tungsten oxide species in the 20 wt% sample. The amounts of these two kinds of acid sites decrease slightly for the 30 wt% sample, possibly due to the weak interaction between the tungsten species and silica, because high contents of tungsten species may lead to the partial collapse of the mesoporous structure and the appearance of crystalline WO_3. Based on the FT-IR spectra after pyridine adsorption, it can be concluded that both the Lewis and Brønsted acid sites evidenced over the tungsten-doped SBA-15 samples are related to tungsten oxide incorporation and that the strong Lewis and Brønsted acid sites are essential to the selective oxidation of CPE.

3.1.5. XPS

Fig. 5 shows the W_{4f} XPS spectra of the W-doped SBA-15 samples. All of the samples demonstrate a broad XPS peak, but it is possible to distinguish tungsten oxide species in different chemical states from the position of the W_{4f} level by the curve-fitting procedure according to the theory of Doniach and Sunjic [46]. Detailed quantitative results from the peak-fitting results of W_{4f} and Si_{2p} are also given in Table 1. The quantitative surface composition results for tungsten-doped SBA-15 samples before and after 15 min Ar^+ etching are also included to explore the differences in composition between the top surface and the subsurface of the samples. The measured spectra appear similar for all samples and show identical positions for the W_{4f} peaks, except for the minor charging effect observed and corrected according to the contaminant carbon (C_{1s} = 284.6 eV). Both W(VI) and W(V) species at $W_{4f_{7/2}}$ (of 36.6 and 34.6 eV [47–49]) for the W_{4f} spin–orbit components are detected. With increasing tungsten oxide loading, the intensity of the W_{4f} XPS peaks also increases before and after Ar^+ etching, as illustrated by the changes in relative peak areas for W_{4f} as shown in Fig. 5 and Table 1. Table 1 also gives the quantitative results of the molar ratios of W^{6+}/W^{5+} and Si/W by XPS according to the relative peak intensity of W_{4f} and Si_{2p} after correction with atomic sensitivity factors. The molar ratio of W^{6+}/W^{5+} increases from 1.9 to 2.2 when the WO_3 contents increases from

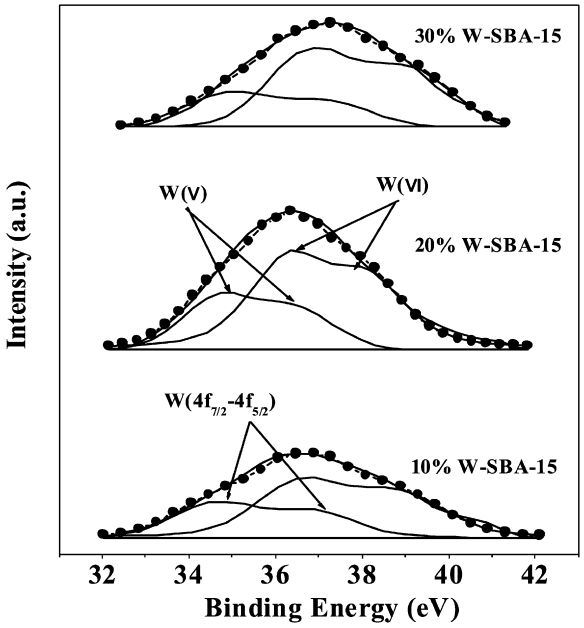

Fig. 5. XPS spectra of the W_{4f} region for different W-doped SBA-15 samples.

Table 1
Peak-fitting results of W_{4f} XPS spectra of W-doped SBA-15 samples

Sample	Binding energy for W_{4f} (eV)				W^{6+}/W^{5+} [a]	Si/W [b]	Si/W [c]
	W^{6+} $W_{4f_{5/2}}$	W^{6+} $W_{4f_{7/2}}$	W^{5+} $W_{4f_{5/2}}$	W^{5+} $W_{4f_{7/2}}$			
WO_3 [d]	38.0	36.0	–	–	–	0	0
$WO_{2.5}$ [d]	–	–	36.8	35.0	–	0	0
10% WO_3-SBA-15	38.9	36.6	36.9	34.6	1.9	107.6	38.6
10% WO_3-SBA-15 [e]	39.2	36.9	36.9	34.6	0.9	106.2	–
20% WO_3-SBA-15	38.9	36.6	36.9	34.6	2.0	59.2	19.3
20% WO_3-SBA-15 [e]	39.1	36.8	36.9	34.6	0.9	57.6	–
30% WO_3-SBA-15	39.1	36.8	37.2	34.9	2.2	53.4	12.8
30% WO_3-SBA-15 [e]	38.9	36.6	36.9	34.6	1.0	51.2	–

[a] Calculated according to the curve-fitting results of the W_{4f} XPS spectra of catalysts.
[b] Calculated according to the peak areas of W_{4f} and Si_{2p}.
[c] Stoichiometric ratio in gel.
[d] See reference: Appl. Catal. A Gen. 269 (2004) 169–177.
[e] After Ar^+ etching for 15 min.

Table 2
Influence of the calcination temperature on the catalytic performance of 20% WO_3-SBA-15[a]

Temperature (K)	Conversion (%)		TOF (h^{-1})	Selectivity (%)		Yield of GA (%)
	Of H_2O_2	Of CPE		GA	CPDL	
673	71	85	1.9	83	12	70
773	91	100	2.2	91	4	91
873	96	100	2.2	87	6	87
973	98	99	2.2	86	7	85
1073	93	91	2.0	85	9	77

[a] Reaction conditions: The molar ratio of CPE:H_2O_2:WO_3 = 100:210:4, the volume ratio of TBP/CPE = 7.5, reaction temperature 308 K, reaction time 12 h. CPE, cyclopentene; GA, glutaraldehyde; CPDL, cyclopentan-1,2-diol; TOF = moles of CPE per moles of WO_3 per hour.

10 to 30%, suggesting that the surface W^{6+} species content increases and much more crystalline WO_3 species are formed in the 30 wt% tungsten-doped SBA-15 sample. However, after 15 min of Ar^+ etching, the W^{6+}/W^{5+} molar ratio of the various samples changes to about half of the initial value, demonstrating that the W^{6+} species are located mainly on the surface of the samples and can be removed by 15 min of Ar^+ etching (also shown in Table 1). At the same time, the existence of highly polymeric tungsten species in the 30 wt% sample leads to the obvious decrease of the Si/W molar ratio compared with the 10 wt% sample, in which the tungsten species are highly dispersed. According to the comparison of the surface molar ratio of W/Si with that of the mean value as added, it can be concluded that the increase of this ratio with the increasing weight percentage of tungsten is not linear. This suggest that the dispersion of the surface tungsten species is not uniform with increasing tungsten loading and that the deviation from linearity is obtained between the sample at WO_3 content >20%.

3.2. Catalytic activity tests in the selective oxidation of CPE to GA

In an earlier research note [22], we briefly reported that the heterogeneous tungsten-doped SBA-15 catalyst exhibited excellent activity and selectivity for the selective oxidation of CPE to GA in a nonaqueous H_2O_2/TBP system. The nonaqueous H_2O_2/TBP system has several advantages over the aqueous H_2O_2/*t*-BuOH system: (1) the very high yield of GA significantly decreases the cost of the raw material; (2) the yield of the main byproduct, cyclopentane-1,2-diol, is only 4%, which can be easily separated from the mixture by distillation; (3) the heterogeneous catalyst can be conveniently separated from the products by simple filtration; (4) GA with high purity (Medical Grade) can be easily obtained through decompressed rectification, due to the large difference in boiling point between GA and TBP (∼100 °C). According to the previous results, we know that the 20 wt% WO_3-SBA-15 catalyst shows the best catalytic performance. The CPE conversion and GA selectivity reach 100% and 91%, respectively. In the present work, the effects of catalyst preparation parameters and reaction conditions on the catalytic performance of 20 wt% WO_3-SBA-15 catalyst in the anhydrous H_2O_2/TBP system were investigated in detail.

Table 3
Influence of the reaction temperature over 20% WO_3-SBA-15[a]

Temperature (K)	Reaction time (h)	Conversion (%)		TOF (h^{-1})	Selectivity (%)		Yield of GA (%)
		Of H_2O_2	Of CPE		GA	CPDL	
298	16	90	97	1.5	86	7	83
308	12	91	100	2.2	91	4	91
318	8	91	100	3.3	83	11	83

[a] Reaction conditions: The molar ratio of CPE:H_2O_2:WO_3 = 100:210:4, the volume ratio of TBP/CPE = 7.5; TOF = moles of CPE per moles of WO_3 per hour.

A reasonable correlation of the structural parameters with its catalytic activity and the reaction mechanism is proposed.

3.2.1. Effect of the calcination temperature

The effect of calcination temperature on the catalytic behaviors of the 20% WO_3-SBA-15 catalyst is shown in Table 2. The catalyst exhibits its best activity and selectivity to GA at 773 K. Calcination temperatures above or below 773 K lead to decreased activity. The TOF values (also shown in Table 2) unambiguously verify the above conclusion, but it should be noted that although the TOF value at 873 K is the same as that at 773 K, the GA yield is slightly decreased at 873 K. These results can be explained based on the XRD characterization, because no significant crystallization is observed at calcination temperatures of 773 K and lower, while the catalyst gradually crystallized with the increase in calcination temperature from 773 to 1073 K (see the supporting materials). Thus, 773 K is chosen as the optimum calcination temperature for the 20 wt% WO_3-SBA-15 catalyst, because the tungsten oxide species could not be fully activated at lower calcination temperature. Moreover, the interaction between tungsten oxide species and the silica framework is not sufficiently strong to effectively inhibit leaching of the active species during the reaction, whereas the significant crystallization of the tungsten oxides species occurs at higher calcination temperature, leading to the poor dispersion of the active species and decreased catalytic performance.

3.2.2. Influence of the reaction parameters

Table 3 shows the effect of the reaction temperature on the catalytic performance of the 20 wt% WO_3-SBA-15 catalyst at 298–318 K. The catalytic performance strongly depends on the reaction temperature. At 298 K, CPE conversion is only 97% after 16 h of reaction, but at 308 K, 100% CPE conversion and 91% GA yield are obtained after only 12 h. A further increase in reaction temperature to 318 K further accelerates the reaction rate, as also confirmed by the TOF values (shown in Table 3), but also increases the byproduct yield. This is because the selective oxidation of CPE is an exothermic reaction, and thus high conversion is expected if the reaction is carried out at high temperature, which would be favorable for the equilibrium conversion to the products. Although high reaction temperature could shorten the reaction time, the aldehyde group of GA is so active that it can be further oxidized at higher temperature, which is possibly more beneficial to formation of the byproducts cyclopentane-1,2-diol (CPDL). All of the above results

Table 4
Effect of catalyst amount on the GA preparation over 20% WO_3-SBA-15[a]

WO_3/CPE (mol%)	Conversion (%)		TOF (h^{-1})	Selectivity (%)		Yield of GA (%)
	Of H_2O_2	Of CPE		GA	CPDL	
1.9	70	73	3.2	86	6	63
2.8	84	95	2.8	89	5	85
3.8	91	100	2.2	91	4	91
4.7	90	100	1.8	90	4	90

[a] Reaction conditions: The molar ratio of CPE:H_2O_2 = 100:210, the volume ratio of TBP/CPE = 7.5, reaction temperature 308 K, reaction time 12 h; TOF = moles of CPE per moles of WO_3 per hour.

Table 5
Effect of TBP amount on the GA preparation over 20% WO_3-SBA-15[a]

TBP/CPE[b]	Conversion (%)		TOF (h^{-1})	Selectivity (%)		Yield of GA (%)
	Of H_2O_2	Of CPE		GA	CPDL	
15.9	61	63	1.4	77	6	49
9.6	90	93	2.0	86	7	79
7.5	91	100	2.2	91	4	91
5.6	89	100	2.2	86	8	86
4.7	89	100	2.2	84	8	84

[a] Reaction conditions: The molar ratio of CPE:H_2O_2:WO_3 = 100:210:4, reaction temperature 308 K, reaction time 12 h.

[b] The volume ratio of TBP/CPE; TOF = moles of CPE per moles of WO_3 per hour.

suggest that an optimum temperature (i.e., 308 K) is necessary for the selective oxidation of CPE to GA, taking into account the balance between the reaction rate and the equilibrium problem.

The reaction results as a function of the amounts of the 20 wt% WO_3-SBA-15 catalyst used were also investigated (see Table 4). It was found that the CPE conversion increases with increasing amounts of catalyst used in the oxidative reaction in a fixed reaction period, suggesting that the reaction rate is accelerated with increasing amounts of catalysts. However, the TOF values decrease significantly with the increment of the catalyst amounts. Moreover, the yield of GA first increases significantly when the molar ratio of WO_3/CPE increases from 1.9 to 3.8%, then decreases slightly when the molar ratio of WO_3/CPE further increases from 3.8 to 4.7%, which may be ascribed to the increased difficulty of mass transfer during the reaction.

Because the solvent is known to play a very important role in determining the catalytic activity and selectivity in many catalytic oxidations by hydrogen peroxide [50], we investigated the effect of the relative amount of TBP on the catalytic performance of the 20% WO_3-SBA-15 catalyst during the CPE oxidation to GA. As shown in Table 5, an appropriate amount of TBP is required for this reaction. When using small amounts of TBP, hydrogen peroxide apparently decomposes during the reaction, releasing heat and leading to volatilization of the reagents. Using more TBP leads to low reagent concentrations and thus decreased reaction rate. The TOF values further demonstrate these results; the TOF values first decrease slightly when the volume ratio of TBP to CPE is increased from 4.7 to 9.6, then decrease significantly when the volume ratio is further increased from 9.6 to 15.9. Based on the experimental data, the optimal volume ratio of TBP to CPE is determined to be 7.5:1.

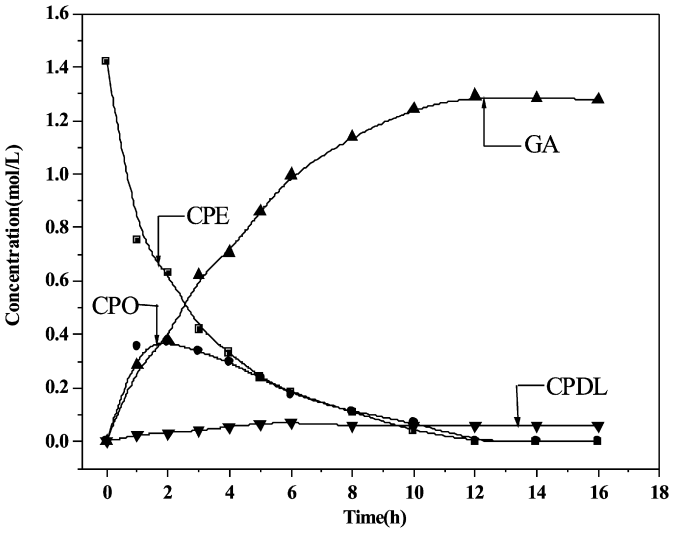

Fig. 6. Dependence of distribution of CPE and the products on the reaction time over 20% WO_3-SBA-15. CPE, cyclopentene; CPO, cyclopentene-epoxide; GA, glutaraldehyde; CPDL, cyclopentan-1,2-diol.

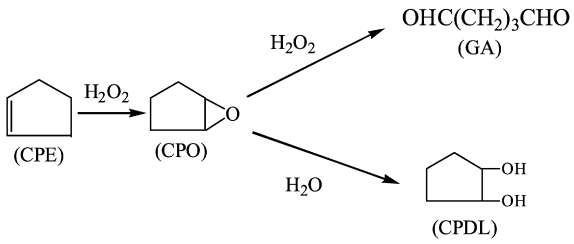

Scheme 1. The catalytic reaction route of CPE oxidation.

3.2.3. The time course of CPE oxidation

According to the GC–MS analysis, along with the main product GA, the main byproducts are cyclopentene-epoxide (CPO) and CPDL. The dependence of the contents of various products on the reaction time over the 20 wt% WO_3-SBA-15 catalyst is illustrated in Fig. 6. The contents of GA increase and reach a maximum at CPE conversion of 100% with about 12 h of reaction time. The GA content remains almost the same with further increases in reaction time. CPO content increases rapidly at the beginning and then decreases progressively with increasing GA content; thus, it can be proposed that CPO is possibly a main intermediate from which GA is produced via its further oxidative cleavage and CPDL is formed via its further reaction with water. Therefore, the mechanism of CPE oxidation in the anhydrous H_2O_2/TBP system may be similar to that in the aqueous H_2O_2/*t*-BuOH system [51]; a possible reaction route is shown in Scheme 1.

3.2.4. Reusability and regeneration of the 20 wt% WO_3-SBA-15 catalyst

To investigate the stability and duration of active tungsten species in the 20 wt% WO_3-SBA-15 catalyst, the leaching of WO_x species into the reaction mixture and the tungsten remain-

Table 6
Reusability and regeneration of 20 wt% WO_3-SBA-15[a]

Entry	Conversion (%)		Yield of GA (%)	Selectivity of GA (%)
	Of H_2O_2	Of CPE		
1	91	100	91	91
2	90	100	88	89
3	89	97	84	86
4	90	95	81	85
5	89	93	79	85
6	85	90	75	84
7[b]	93	100	90	90

[a] Reaction time 12 h, reaction temperature 308 K, the molar ratio of CPE: H_2O_2:WO_3 = 100:210:4, the volume ratio of TBP/CPE = 7.5.
[b] After regeneration.

ing in the catalyst were determined by ICP analyses after six reaction cycles. No detectable leaching of W-species or obvious loss of tungsten in the 20 wt% WO_3-SBA-15 catalyst can be seen, demonstrating the presence of strong interactions between active tungsten species and the silica-based matrix with SBA-15 structure. A similar phenomenon was also reported by Somma et al. [52] when using niobium-based catalyst in the epoxidation of olefins with hydrogen peroxide. The results of the selective oxidation of CPE to GA over the 20 wt% WO_3-SBA-15 catalyst with different reaction cycles and the postregeneration material are also listed in Table 6. The GA yield decreases slowly and remains above 80% even after the sixth cycle. However, after calcination at 773 K in air for 2 h, the outstanding catalytic activity could be recovered. In addition, small amounts of contaminant carbon are detected by XPS on the surface of the used 20 wt% WO_3-SBA-15 catalyst and can be easily removed with calcination at 773 K in air for 2 h. Therefore, the surface contaminant carbon, which must result in the decrease of the active centers, is the main reason for the decreased GA yield during the recycling of the 20 wt% WO_3-SBA-15 catalyst. In conclusion, the 20 wt% WO_3-SBA-15 catalyst shows high stability and activity for the selective oxidation of CPE to GA and can be regenerated by simple calcination in air.

3.2.5. Comparison of catalytic performance over different catalysts in the anhydrous H_2O_2/TBP system

In earlier studies, we addressed the catalytic performance of titania-supported tungsten oxide catalyst (the mesoporous core–shell structured WO_3/TiO_2 spheroid), which showed good catalytic activity for the selective oxidation of CPE to GA in the aqueous H_2O_2/*t*-BuOH system [15]. For comparison, we also investigated its catalytic performance in the anhydrous H_2O_2/TBP system. The results show that the CPE conversion is 97% and GA yield is only 72% over the 20 wt% WO_3/TiO_2 spheroid catalyst at 308 K for 24 h, much lower than the values on 20 wt% W-doped SBA-15 catalysts. Moreover, much more cyclopentene oxide is formed on the WO_3/TiO_2 spheroid catalyst (ca. 15%), suggesting that titania-supported tungsten has weaker redox ability compared with the silica-based catalyst, on which deep oxidation is apt to occur. All of these results indicate that both the nature and the structure of the support for the WO_3-based catalyst strongly influence the catalytic activity and selectivity in the title reaction. First, the mesoporous SBA-15 material has low intrinsic catalytic activity due to the amorphous nature of the pore walls. Thus, the tungsten oxide species in the W-doped SBA-15 catalysts are the active centers. Titania-based catalysts have intrinsic redox activity for the selective oxidation of a large family of organic molecules using hydrogen peroxide as an oxidant; but only cyclopentene oxide is obtained when mesoporous TiO_2–SiO_2 material is used as the catalyst. Thus, it may be concluded that tungsten oxide species in the WO_3/TiO_2 spheroid catalysts cause the further oxidation of cyclopentene oxide. Second, the pure siliceous material has a higher surface area and a more uniform mesoporous structure; as a result, WO_3 species are highly dispersed in the tungsten-doped SBA-15 catalyst and the mesoporous structure entails more agitated flow, which then increases the interaction possibility between reactants and catalytic active centers.

3.3. Surface state of tungsten species

This work has investigated a novel WO_3-SBA-15 catalyst prepared by the in situ method for the selective oxidation of CPE to GA in the anhydrous H_2O_2/TBP system. Previously reported results demonstrate that incorporating tungsten into mesoporous SBA-15 material by the in situ synthesis method allows the greater dispersion of tungstic species into the siliceous matrix compared with the conventional impregnation method, leading to an improved selectivity to GA during the selective oxidation of CPE [22]. Moreover, the tungsten-doped SBA-15 catalyst shows much higher catalytic performance in the anhydrous H_2O_2/TBP system than in the aqueous H_2O_2/*t*-BuOH system.

This work also has investigated the nature and redox properties of the W-doped SBA-15 catalysts in the anhydrous system. The UV–vis DRS results demonstrate that at low tungsten oxide content ($\leqslant$20 wt%), the tungsten-doped SBA-15 catalyst consists mainly of highly dispersed tetrahedral tungsten oxide species and low-condensed oligomeric tungsten oxide entities. At higher tungsten oxide loading, polymeric tungsten oxide species become abundant, and bulk WO_3 species appear. The TPR results further confirm that the isolated tetrahedral coordination or the low-condensed oligomeric tungsten oxide species are more difficult to reduce, which are predominant in catalysts with low tungsten oxide content. The reducibility of high polymeric tungsten oxide species and WO_3 crystallites, formed on the surface of the catalysts with tungsten oxide content $>$20 wt%, is similar to that of bulk WO_3. UV–vis DRS and TPR characterizations of the catalysts demonstrate that the tungsten species in the WO_3-SBA-15 catalyst are highly dispersed at low tungsten oxide content and that there are strong interactions between the tungsten species and the support, preventing leaching of the tungsten species during the selective oxidation of CPE to GA with the anhydrous hydrogen peroxide. Compared with the visible Raman spectra reported in our earlier work [22], the present UV-Raman spectra show significant different results regarding the structure of the tungsten oxide species. The terminal W=O bond suggested as the active sites of the tungsten-based catalyst is seen in a band at about 970 cm^{-1}. The Raman band at about 900 cm^{-1} associated with the Si–O–W bond demon-

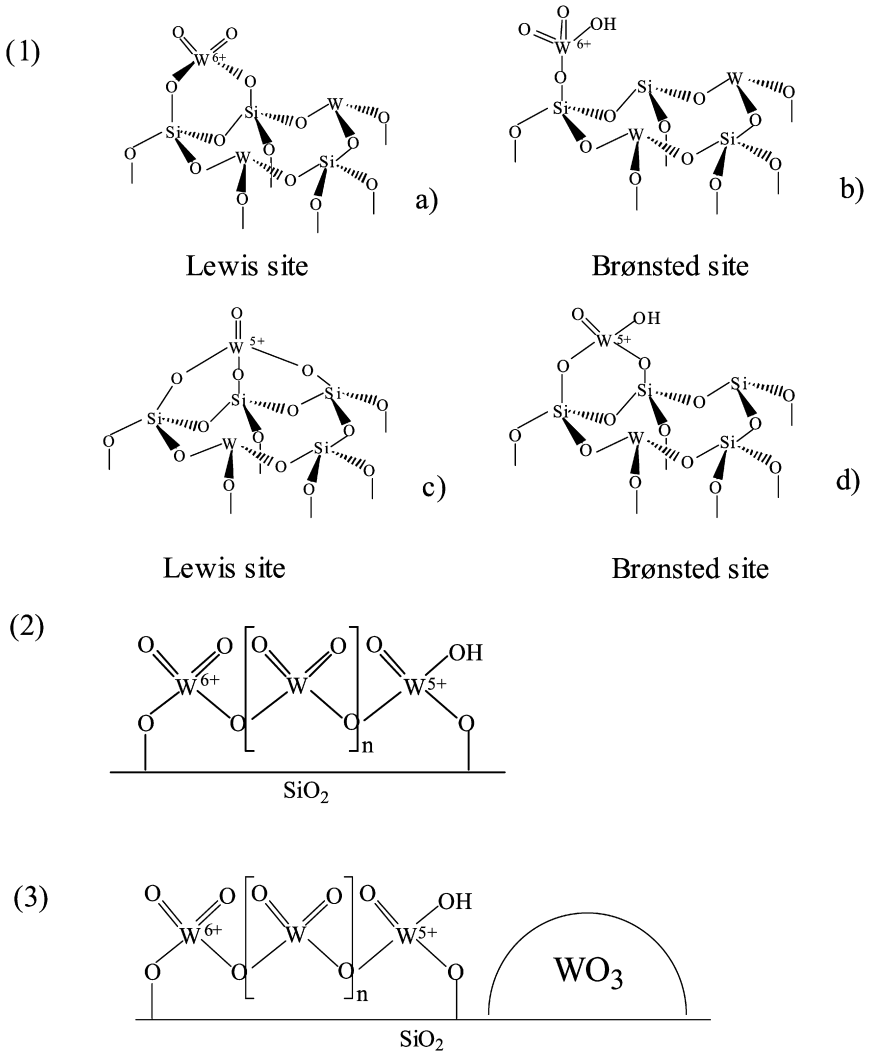

Fig. 7. Proposed models of the structure of the tungsten oxide species in the W-doped SBA-15 catalyst.

strates that parts of tungsten oxide species are incorporated into the SBA-15 framework. The existence of the Raman band at 685 cm^{-1} assigned to stretching and bending modes of W–O bonds may indicate the presence of low-condensed polymeric WO_x species. Investigation by means of XPS has confirmed that two types of tungsten oxide with oxidation states of 6+ and 5+ are present in the W-doped SBA-15 catalyst. The content of high-oxidation tungsten (W^{6+}) increases with the increment of tungsten oxide content, suggesting the conglomeration degree of tungsten oxide species increases and finally bulk WO_3 appears in the 30 wt% WO_3-SBA-15 catalyst. Characterization by Py-FT-IR has confirmed the formation of acidic Brønsted sites and the generation of new Lewis acid sites over the tungsten-doped SBA-15 catalysts. This result indicates that incorporation of tungsten into the SBA-15 framework provokes both the Brønsted and Lewis acid sites. Moreover, pyridine desorption at different temperatures reveals that a proper content ($\leqslant$20 wt%) is essential to provoking the strong Brønsted and Lewis acid sites.

Our detailed investigation of the catalytic performance of the W-doped SBA-15 catalysts shows that the 20 wt% WO_3-SBA-15 catalyst exhibits the best activity (100% CPE conversion) and selectivity (91% GA yield) in the selective oxidation of CPE to GA in the anhydrous system. Based on the characterization results presented above, it can be concluded that proper content of tungsten oxide species and its high dispersion account for its high activity and the polymerization degree of the active tungsten oxide species has a significant effect on the catalytic behavior of the tungsten-doped SBA-15 catalysts. The isolated and the low-condensed oligomeric tungsten oxide species show high activity and selectivity for the selective oxidation of CPE to GA, whereas the appearance of WO_3 crystallites decreases the catalytic performance of the catalysts. In addition, the TOF values for the W-doped SBA-15 catalysts with different WO_3 contents might be considered to account for the above results. The TOF values first increase at WO_3 content $<$20 wt% (at which the tungsten oxide species exhibit a highly dispersed nature), then decrease at WO_3 content $>$20 wt% due to the formation of WO_3 crystallites [22]. Thus, the nature and structure of the tungsten oxide species strongly depend on tungsten oxide content, as shown in Fig. 7. As shown in Fig. 7(1), the isolated tungsten oxide species in the tetra-

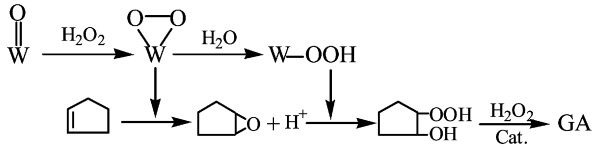

Scheme 2. Proposed mechanism of the selective oxidation of CPE to GA.

hedral coordination possibly can be divided into four kinds of structures that show high activity in the title reaction. Increasing the tungsten oxide content leads to the formation of polymeric species (Fig. 7(2)), which also shows high activity at low condensed oligomers. Finally, with increasing polymerization degree of the tungsten oxide species, the bulk WO_3 species appear, as shown in Fig. 7(3). We know that the terminal W=O group is suggested as the active site and cyclopentene-epoxide is the main intermediate, therefore, the possible reaction mechanism of CPE oxidation can be reasonably simplified as Scheme 2, which involves epoxidation of CPE, conversion of cyclopentene-epoxide into β-hydroxycyclopentylperoxide, and rearrangement of β-hydroxycyclopentylperoxide into GA according to the studies on the mechanism of the title reaction in the homogeneous catalytic system [53,54]. Detailed work on the mechanism at the molecular level is currently underway.

4. Conclusion

This paper presents a detailed study of the structure of tungsten oxide doped in the mesoporous SBA-15 materials and its catalytic properties in the selective oxidation of CPE to GA. Various characterization results prove that the as-synthesized material shows a typical structure of SBA-15. WO_x species are highly dispersed into the lattice of the bulk and might be imbedded separately at low tungsten oxide content, possibly serving as the active centers for the selective oxidation of CPE to GA. TPR results shows a strong interaction between WO_x species and the siliceous SBA-15 matrix, which could effectively prevent the active species from leaching into the reaction mixture. The FT-IR-pyridine adsorption experiment confirms the presence of strong Brønsted acid and Lewis acid sites on incorporating tungsten oxide species into the SBA-15 materials, enhancing catalytic performance. The optimal tungsten content is 20 wt%, and the GA yield over this catalyst reaches 91%, suggesting its promising potential use in industry.

Acknowledgments

This work was supported by the Major State Basic Resource Development Program (grant 2003CB615807), NSFC (projects 20407006 and 20573024), and the Natural Science Foundation of Shanghai Science & Technology Committee (grant 06JC14004). The authors thank Professor Heyong He for his kind help in improving the English, Professor Yong Cao for assistance with the UV-Raman experiments, and Professor Hexing Li for useful discussions.

Supporting materials

The online version of this article contains additional supporting materials.

Please visit DOI: 10.1016/j.jcat.2007.05.002.

References

[1] C.T. Kresge, M.E. Leonowicz, W.J. Roth, J.C. Vartuli, J.C. Beck, Nature 359 (1992) 710.
[2] D.Y. Zhao, J.L. Feng, Q.S. Huo, N. Melosh, G.H. Fredrickson, B.F. Chmelka, G.D. Stucky, Science 279 (1998) 548.
[3] J.S. Beck, J.C. Vartuli, W.J. Roth, M.E. Leonowicz, C.T. Kresge, K.D. Schmitt, C.T.W. Chu, D.H. Olsen, E.W. Sheppard, S.B. Mccullen, J.B. Higgins, J.L. Schlenker, J. Am. Chem. Soc. 114 (1992) 10834.
[4] Z. Luan, M. Hartmann, D. Zhao, W. Zhou, L. Kevan, Chem. Mater. 11 (1999) 1621.
[5] P. Wuy, T. Tatsumi, T. Komatsu, T. Yashima, Chem. Mater. 14 (2002) 1657.
[6] Z. Luan, J.Y. Bae, L. Kevan, Chem. Mater. 12 (2000) 3202.
[7] P. Shah, A.V. Ramaswamy, K. Lazar, V. Ramaswamy, Appl. Catal. A Gen. 273 (2004) 239.
[8] R.D. Wilson, D.G. Barton, C.D. Baertsch, E. Iglesia, J. Catal. 194 (2000) 175.
[9] B.F. Sels, D.E. De Vos, P.A. Jacobs, Angew. Chem. Int. Ed. 44 (2) (2005) 310.
[10] C.D. Baertsch, K.T. Komala, Y.H. Chua, E. Iglesia, J. Catal. 205 (2002) 44.
[11] T. Kabe, W.H. Qian, A. Funato, Y. Okoshi, A. Ishihara, Phys. Chem. Chem. Phys. 5 (1999) 921.
[12] Y. Rezgui, M. Guemini, Appl. Catal. A Gen. 282 (2005) 45.
[13] U. Ciesla, D. Demuth, R. Leon, P. Petroff, G. Stucky, K. Unger, F. Schüth, J. Chem. Soc. Chem. Commun. (1994) 1387.
[14] M.J. Yuan, Z. Shan, B.Z. Tian, B. Tu, P.Y. Yang, D.Y. Zhao, Microporous Mesoporous Mater. 78 (2005) 37.
[15] X.L. Yang, W.L. Dai, C.W. Guo, H. Chen, Y. Cao, H.X. Li, H.Y. He, K.N. Fan, J. Catal. 234 (2005) 438.
[16] C. Martín, P. Malet, G. Solana, V. Rives, J. Phys. Chem. B 102 (1998) 2759.
[17] F. Somma, G. Strukul, J. Catal. 227 (2004) 344.
[18] Z.R. Zhang, J.S. Sue, X.M. Zhang, S.B. Li, Chem. Commun. (1998) 241.
[19] E. Briot, J.Y. Piquemal, M. Vennat, J.M. Brégeault, G. Chottard, J.M. Manoli, J. Mater. Chem. 10 (2000) 953.
[20] W.L. Dai, H. Chen, Y. Cao, H.X. Li, S.H. Xie, K.N. Fan, Chem. Commun. (2003) 892.
[21] J.E. Herrera, J.H. Kwak, J.Z. Hu, Y. Wang, C.H.F. Peden, J. Macht, E. Iglesia, J. Catal. 239 (2006) 200.
[22] X.L. Yang, W.L. Dai, H. Chen, Y. Cao, H.X. Li, H.Y. He, K.N. Fan, J. Catal. 229 (2005) 259.
[23] H. Furukawa, E. Nishikawa, T. Koyama, JP Patent 6,219,546 (1987).
[24] J.F. Deng, X.H. Xu, H.Y. Chen, A.R. Jiang, Tetrahedron 48 (1992) 3503.
[25] W.Z. Weng, M.S. Chen, Q.G. Yan, T.H. Wu, Z.S. Chao, Y.Y. Liao, H.L. Wan, Catal. Today 63 (2000) 317.
[26] H. Chen, W.L. Dai, J.F. Deng, K.N. Fan, Catal. Lett. 81 (2002) 131.
[27] A. Stein, M. Fendorf, T.P. Jarvie, K.T. Mueller, A.J. Benesi, T.E. Mallouk, Chem. Mater. 7 (1995) 304.
[28] Y. Wand, O. Zhang, Y. Ohishi, T. Shishido, K. Takehira, Catal. Lett. 72 (2001) 215.
[29] C.W.F.T. Pistorius, J. Chem. Phys. 44 (1966) 4532.
[30] O. Klepel, W. Böhlmann, E.B. Ivanov, V. Riede, H. Papp, Microporous Mesoporous Mater. 76 (2004) 105.
[31] R.S. Weber, J. Catal. 151 (1995) 470.
[32] E. Iglesia, D.G. Barton, S.L. Soled, S. Miseo, J.E. Baumgartner, W.E. Gates, G.A. Fuentes, G.D. Meitzner, Stud. Surf. Sci. Catal. 101 (1996) 533.

[33] C. Li, G. Xiong, Q. Xin, J.K. Liu, P.L. Ying, Z. Feng, J. Li, W.B. Yang, Y.Z. Wang, G.R. Wang, X.Y. Liu, M. Lin, X.Q. Wang, E.Z. Min, Angew. Chem. Int. Ed. 38 (1999) 2220.
[34] G. Xiong, C. Li, H. Li, Q. Xin, Z. Feng, Chem. Commun. (2000) 677.
[35] F. Figueras, J. Palomeque, S. Loridant, C. Fèche, N. Essayem, G. Gelbard, J. Catal. 226 (2004) 25.
[36] L. Salvatl Jr., L.E. Makovsky, J.M. Stencel, F.R. Brown, D.M. Hercules, J. Phys. Chem. 85 (1981) 3700.
[37] A. de Lucas, J.L. Valverde, P. Cañizares, L. Rodriguez, Appl. Catal. A Gen. 184 (1999) 143.
[38] X.T. Gao, S.R. Bare, B.M. Weckhuysen, I.E. Wachs, J. Phys. Chem. B 102 (1998) 10842.
[39] J.Y. Piquemal, E. Briot, M. Vennat, J.M. Brégeault, G. Chottardb, J.M. Manoli, Chem. Commun. (1999) 1195.
[40] D.C. Vermaire, P.C. Vanberge, J. Catal. 116 (1989) 309.
[41] D.G. Barton, S.L. Soled, G.D. Meitzner, G.A. Fuentes, E. Iglesia, J. Catal. 181 (1999) 57.
[42] L. Karakonstantis, H. Matralis, Ch. Kordulis, A. Lycourghiotis, J. Catal. 162 (1996) 306.
[43] J.A. Horsley, I.E. Wachs, J.M. Brown, G.H. Via, F.D. Hardcastle, J. Phys. Chem. 91 (1987) 4014.
[44] A. de Lucas, J.L. Valverde, P. Caňizares, L. Rodriguez, Appl. Catal. A Gen. 172 (1998) 165.
[45] I.E. Wachs, Catal. Today 27 (1996) 437.
[46] S. Doniach, M. Sunjic, J. Phys. Chem. 3 (1970) 285.
[47] F. Le Normand, J. El Fallah, L. Hilaire, P. Lègarè, A. Kotani, J.C. Parlebas, Solid State Commun. 71 (1989) 885.
[48] M. Valigi, D. Gazzoli, I. Pettiti, G. Mattei, S. Colonna, S. De Rossi, G. Ferraris, Appl. Catal. A Gen. 231 (2002) 159.
[49] E. Salje, A.F. Carley, M.W. Roberts, J. Solid State Chem. 29 (1979) 237.
[50] V. Hulea, E. Dumitriu, F. Patcas, R. Ropot, P. Graffin, P. Moreau, Appl. Catal. A Gen. 170 (1998) 169.
[51] R.H. Jin, H.X. Li, J.F. Deng, J. Catal. 203 (2001) 75.
[52] F. Somma, P. Canton, G. Strukul, J. Catal. 229 (2) (2005) 490.
[53] W.L. Dai, X.J. Huang, H.Y. Chen, J.F. Deng, Indian J. Chem. Sect. B 36 (1997) 583.
[54] Y. Lu, H.B. Yin, H.X. Wu, H. Liu, T.S. Jiang, Y.J. Wada, Catal. Commun. 7 (2006) 832.